FOURTH-ORDER STATISTICS FOR PARAMETER ESTIMATION

E. Lima, L. T. Santos, J. Schleicher and M. Tygel

email: *mtygel@gmail.com*
keywords: *Semblance, moments, CMP, CRS*

ABSTRACT

Semblance is the mostly used coherence measure for parameter estimation from geophysical data. The best example is velocity analysis in which the normal-moveout velocity is extracted from common-midpoint (CMP) gathers. In complete analogy to velocity analysis, semblance is also applied to estimate Common-Reflection-Surface (CRS) parameters by means of the hyperbolic traveltime applied to multicoverage data. In statistics, semblance is related to the so-called second moment and in optimization theory, to the least-squares solution of maximum signal energy as a characterization of reflection events. Extensions of the usual semblance can be defined by replacing second-order by higher-order quantities. Here we found encouraging results by a natural extension of semblance to fourth order. The introduced fourth-order semblance is applied to CRS parameter estimation. Numerical examples show that the search using fourth-order semblance is more reliable for high noise levels.

INTRODUCTION

Since the famous work of Taner and Koehler (1969), semblance has been a reliable measure of coherence in seismic processing. Many applications like stacking velocity analysis (Doherty and Claerbout, 1976; Yilmaz, 1979), migration velocity analysis (Sattlegger, 1975; Dohr and Stiller, 1975; Al-Yahya, 1989; Schleicher and Biloti, 2007), filter techniques (Reiter et al., 1993) or CRS stack (see, e.g., Höcht et al., 1999) rely on semblance to detect the shape of reflection events in seismic data.

Semblance is known to depend in various degrees on operator size (aperture and window length) and noise level (Douze and Laster, 1979). Moreover, it is based on the assumption of white noise. Therefore, it sometimes shows unpredictable behaviour if the noise is actually coloured. For these reasons, many attempts have been made to find a more stable measure of coherence that depends less on the kind of noise in the data or the choice of the parameters used in the analysis. One of the most successful ones is differential semblance (Symes and Carazzone, 1991; Symes and Kern, 1994).

Being a very robust and easy to calculate measure of coherence for a broad variety of situations, the second-order coherence measure semblance has survived all these attempts. Nonetheless, there exist particular situations, where other coherency measures can be advantageous. In this paper, we compare its behaviour to those of a first- and a fourth-order coherence measure. We show that while in conventional velocity analysis, there is no gain in replacing semblance by one of the other measures, for the linear search of the CRS stack (Müller, 1999), the fourth-order measure is less dependent on aperture and noise level, thus resulting in reliable estimates of the local slope more often than when using conventional semblance.

INTERPRETATION OF SEMBLANCE IN STATISTICS

One important step in the CMP (or CRS) stacking process is to find pre-assigned curves or surfaces (e.g., hyperbolic curves) that fit the reflection traveltimes in some best possible way. Of paramount importance is an accurate determination of the parameters that define the best-fit curves or surfaces, as these con-

vey most relevant information to be extracted from the seismic data. Of course, due to the presence of noise, these tasks can be very difficult. Therefore, it is necessary to have some measure to decide whether some curve/surface fits the traveltimes. One possibility for such a measure is the degree of *alignment or coherence* of the seismic traces along the trial curves/surfaces.

Semblance is a quantitative measure of coherence, typically used for event characterization in noisy data sets, for example seismic data. In a certain sense, semblance represents the energy of the stacked trace divided by the energy sum of all stacking traces within a given time window. Mathematically, semblance is defined as

$$\widetilde{S}_2 = \frac{\displaystyle\sum_{k=-w}^{w} \left(\sum_{i=1}^{N} u_i(t_k) \right)^2}{N \displaystyle\sum_{k=-w}^{w} \left(\sum_{i=1}^{N} u_i(t_k)^2 \right)}. \tag{1}$$

Here, the inner summation represents the traces (index i) along which the stack is performed; the outer summation performs the stack for various time samples (index k), that fall in a given time window of width $2w + 1$. The window width should be related to the length of the signal wavelet of the event. The summation enhances the signal-to-noise ratio of the resulting stack. In order to study semblance as a statistical or optimization concept, it is convenient to disregard the time-window summation. In other words, we shall, for the moment, define the *local semblance* as the simpler expression

$$S_2 = \frac{\left(\displaystyle\sum_{i=1}^{N} u_i \right)^2}{N \displaystyle\sum_{i=1}^{N} u_i^2}. \tag{2}$$

To describe the relationship between local semblance S_2 and statistical quantities, it is convenient to consider, for a given sample $(u_1, u_2, \ldots, u_N)$, the *simple moment of order* m, or simply m*-moment*, μ_m, defined by

$$\mu_m = \frac{1}{N} \sum_{i=1}^{N} u_i^m, \quad m = 0, 1, 2, \ldots. \tag{3}$$

We readily note that $\mu_0 = 1$ and μ_1 is the standard *mean* or *average*. With the help of the above definitions, the local semblance S_2 of equation (2) can be recast as

$$S_2 = \frac{\mu_1^2}{\mu_2}. \tag{4}$$

To generalize the local semblance to a corresponding higher-order quantity (namely in terms of higher-order moments), we introduce the *central* m*-moments*

$$\sigma_m = \frac{1}{N} \sum_{i=1}^{N} (u_i - \mu_1)^m, \quad m = 0, 1, 2, \ldots, \tag{5}$$

for which $\sigma_0 = 1$ and $\sigma_1 = 0$. In particular, σ_2 is called the *variance*, which can be written as

$$\sigma_2 = \mu_2 - \mu_1^2. \tag{6}$$

The various quantities σ_m measure different dispersion attributes about the mean. Roughly speaking, the variance carries information about the concentration of the sample in some interval around the mean. A large value of the variance indicates a disperse distribution. A small variance means that the data is clustered around the mean.

For our purposes, we are only interested in moments of *even* order, in fact for definiteness, fourth order. We observe that the local semblance S_2 is naturally related to the second-order moments (simple and central) by the relationship

$$\sigma_2 = \mu_2 - \mu_1^2 = \mu_2 \left(1 - \frac{\mu_1^2}{\mu_2}\right) = \mu_2(1 - S_2) \tag{7}$$

or, equivalently,

$$S_2 = 1 - \frac{\sigma_2}{\mu_2}. \tag{8}$$

Equation (8) is the key relation that enables us to extend the semblance concept to higher (even) orders. Here, we only consider the fourth order. In analogy to equation (8), we define the fourth-order "local semblance" S_4 as

$$S_4 = 1 - \frac{\sigma_4}{\mu_4} = \frac{\mu_1}{\mu_4}\left(4\mu_3 - 6\mu_1\mu_2 + 3\mu_1^3\right). \tag{9}$$

As our final expression for the fourth-order coherency measure, which will replace the usual (second-order) semblance, we re-introduce the (external) time-window ummation of the original semblance definition in equation (1). Thus, the final fourth-order semblance is defined as

$$\widetilde{S}_4 = \frac{\displaystyle\sum_{k=-w}^{w}\left(\sum_{i=1}^{N} u_i(t_k)\right)\left[4N^2\left(\sum_{i=1}^{N} u_i(t_k)^3\right) - 6N\left(\sum_{i=1}^{N} u_i(t_k)\right)\left(\sum_{i=1}^{N} u_i(t_k)^2\right) + 3\left(\sum_{i=1}^{N} u_i(t_k)\right)^3\right]}{N^3 \displaystyle\sum_{k=-w}^{w}\left(\sum_{i=1}^{N} u_i(t_k)^4\right)}. \tag{10}$$

INTERPRETATION OF SEMBLANCE IN OPTIMIZATION THEORY

As mentioned earlier, semblance is used in the CMP or CRS stack as a measure of cohrerence along a specified trial curve or surface through the seismic data. Let the vector $\mathbf{u} = (u_1, u_2, \ldots, u_N)$ represent the amplitudes along some curve/surface in the seismic section, for some limited aperture around the central point that is being analysed. We may assume that these values must be reasonably constant if they are perfectly coherent, i..e., if they are aligned along the correct traveltime curve/surface. Hence, we can find the N-dimensional constant vector $\mathbf{c} = (x, x, \ldots, x)$ that is "closest" to $\mathbf{u}$ and to use their "distance" as a measure of the fit. There are many different ways to define the distance between N-dimensional vectors $\mathbf{u}$ and $\mathbf{c}$, some of the possibilities being analysed below.

The first possibility is to minimize the average of the absolute values of the differences of the $\mathbf{x}and\mathbf{u}$ components, $|x - u_i|$, namely,

$$\min_x \; R_1(x) \equiv \frac{1}{N}\sum_{i=1}^{N} |x - u_i|. \tag{11}$$

The residual R_1 is known as the *absolute residual* and its value at the mean, $R_1(\mu_1)$, is the well-known *absolute standard deviation*. The solution to equation (11) is given by the *median*, $x^* = \mathcal{M}$, the value that is above (or below) 50% of the values of $\mathbf{u}$. Without loss of generality, we will assume that the elements of $\mathbf{u}$ are in ascending (or descending) order. It is not difficult to see that the median can be computed as,

$$\mathcal{M} = \begin{cases} u_{(N+1)/2} & , \quad N \text{ is odd}, \\ \dfrac{u_{N/2} + u_{N/2+1}}{2} & , \quad N \text{ is even}. \end{cases} \tag{12}$$

The minimal absolute residual is then given by

$$R_1(\mathcal{M}) = \frac{1}{N}\sum_{i=1}^{N} |u_i - \mathcal{M}|, \tag{13}$$

from which we can measure the fit by the expression,

$$S_1 = 1 - \frac{R_1(\mathcal{M})}{R_1(0)}. \tag{14}$$

Clearly, $S_1 \leq 1$, and since $R_1(\mathcal{M})$ is the minimal residual, we also have $S_1 \geq 0$. The less $R_1(\mathcal{M})$ is, the closer to one S_1 will be. In particular, $S_1 = 0$ for $\mathcal{M} = 0$ and $S_1 = 1$ if $\mathbf{u}$ is a constant vector. The main drawback to work with the first-order "semblance" function S_1 is that it is a nondifferentiable function. Moreover, there is no closed form for S_1, in the sense that we need to first compute $\mathcal{M}$ and then compute the residual.

Let us next analyse a second-order type semblance function. It is a well-known result that the mean, $x^* = \mu_1$, is the solution of the quadratic (least-squares) optimization problem,

$$\min_x \; R_2(x) \equiv \frac{1}{N}\sum_{i=1}^{N}(x - u_i)^2. \tag{15}$$

To see this, observe that $(dR_2/dx)(x) = 0$ is equivalent to $\sum_{i=1}^{N}(x - u_i) = 0$. Since $(d^2R_2/dx^2)(x) = 2/N > 0$, the zero of the derivative is the global minimizer. In other words, the mean is the value that minimizes the root-mean-square (RMS) residual, $\sqrt{R_2(x)}$. Substituting $x^* = \mu_1$ in the residual R_2 we find

$$R_2(\mu_1) = \frac{1}{N}\sum_{i=1}^{N}(u_i - \mu_1)^2 = \sigma_2, \tag{16}$$

i.e., the minimal quadratic residual equals the second central moment. As in the previous case, we can define the relative measure of the fit as

$$S_2 = 1 - \frac{R_2(\mu_1)}{R_2(0)} = 1 - \frac{\sigma_2}{\mu_2} = \frac{\mu_1^2}{\mu_2}. \tag{17}$$

Note that this defines the "true" second-order semblance function in correspondence with equations (2), (4), and (8). Observe that, as in the case of the absolute residual, $0 \leq S_2 \leq 1$, with $S_2 = 0$ if $\mu_1 = 0$ and $S_2 = 1$ if $\mathbf{u}$ is a constant vector. The semblance function can also be interpreted as the square of the cosine of the angle θ between the amplitude vector $\mathbf{u}$ and the constant vector $\mathbf{c} = (\mu_1, \mu_1, \ldots, \mu_1)$,

$$\cos^2\theta = \frac{\left(\sum_{i=1}^{N} u_i\ \mu_1\right)^2}{\left(\sum_{i=1}^{N} u_i^2\right)\left(\sum_{i=1}^{N} \mu_1^2\right)} = \frac{\left(N\mu_1^2\right)^2}{(N\mu_2)(N\mu_1^2)} = \frac{\mu_1^2}{\mu_2} = S_2. \tag{18}$$

Increasing the order of the residual to four, let us now consider the optimization problem,

$$\min_x \; R_4(x) \equiv \frac{1}{N}\sum_{i=1}^{N}(x - u_i)^4, \tag{19}$$

i.e., we are now attempting to minimize the fourth-order (quartic) residual. Although the above minimization problem is very similar to its second-order counterpart (15), an explicit optimal solution in this case cannot be easily found. In fact, it involves the solution of the cubic polynomial equation,

$$\frac{dR_4}{dx}(x) = \frac{4}{N}\left(x^3 - 3\mu_1 x^2 + 3\mu_2 x - \mu_3\right) = 0. \tag{20}$$

The unique real solution, $x^* = \kappa$, can be computed using Cardano's formula, but the final expression cannot be easily manipulated. The same applies for the quartic residual function R_4 and the corresponding semblance function. This makes a fourth-order semblance function defined through the deviation of the minimum residual hard to use.

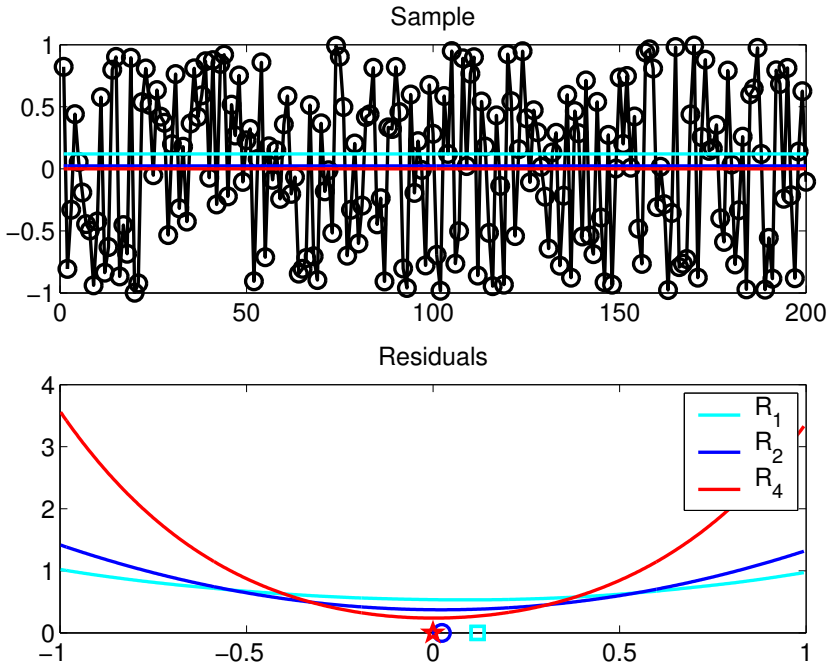

Figure 1: Random sample (top) and the residual functions R_1, R_2 and R_4 (bottom). The horizontal lines in the top figure and the symbols in the bottom one indicate the values of the minimizers of the absolute (R_1), quadratic (R_2) and quartic (R_4) residuals: $\square = \mathcal{M}$, $\bigcirc = \mu_1$ and $\bigstar = \kappa$, respectively.

However, there is another, computationally more appealing way of defining a fourth-order semblance-like function. For this purpose, we replace the optimal quartic residual,

$$R_4(\kappa) = \frac{1}{N}\sum_{i=1}^{N}(u_i - \kappa)^4, \tag{21}$$

by the *quartic residual at the mean*,

$$R_4(\mu_1) = \frac{1}{N}\sum_{i=1}^{N}(u_i - \mu_1)^4 = \sigma_4, \tag{22}$$

which is equal to the fourth-order central moment σ_4. Computing the relative quartic residual, as we have done for the absolute and quadratic residuals, we obtain

$$S_4 = 1 - \frac{R_4(\mu_1)}{R_4(0)} = 1 - \frac{\sigma_4}{\mu_4} = \frac{\mu_1}{\mu_4}\left(4\mu_3 - 6\mu_1\mu_2 + 3\mu_1^3\right), \tag{23}$$

which is the expression for the fourth-order semblance function, S_4. given by equation (9). As in the cases of S_1 and S_2, we also note that $S_4 \leq 1$. However, we cannot ensure that $S_4 \geq 0$, since $R_4(\mu_1)$ is not the minimal quartic residual. In any case, $S_4 = 1$ only if $\mathbf{u}$ is a constant vector, as desirable, and $S_4 = 0$ if $\mu_1 = 0$ as before.

Figure 1 illustrates, for a random number distribution between zero and one, the behavior of the absolute, quadratic and quartic residuals and minimizers. The top part shows the random sample together with its median (first-order minimizer), $\mathcal{M}$, (cyan line), mean (second-order minimizer), μ_1 (blue line), and quartic minimizer κ (red line). The bottom part shows the residual functions R_1 (cyan line), R_2 (blue line), and R_4 (red line) as a function of x, together with their respective minima.

To examine the behavior of the various semblance functions (S_1, S_2 and S_4) in a noisy environment, we calculated their values for the typical amplitude curve after adding different levels of noise. The results

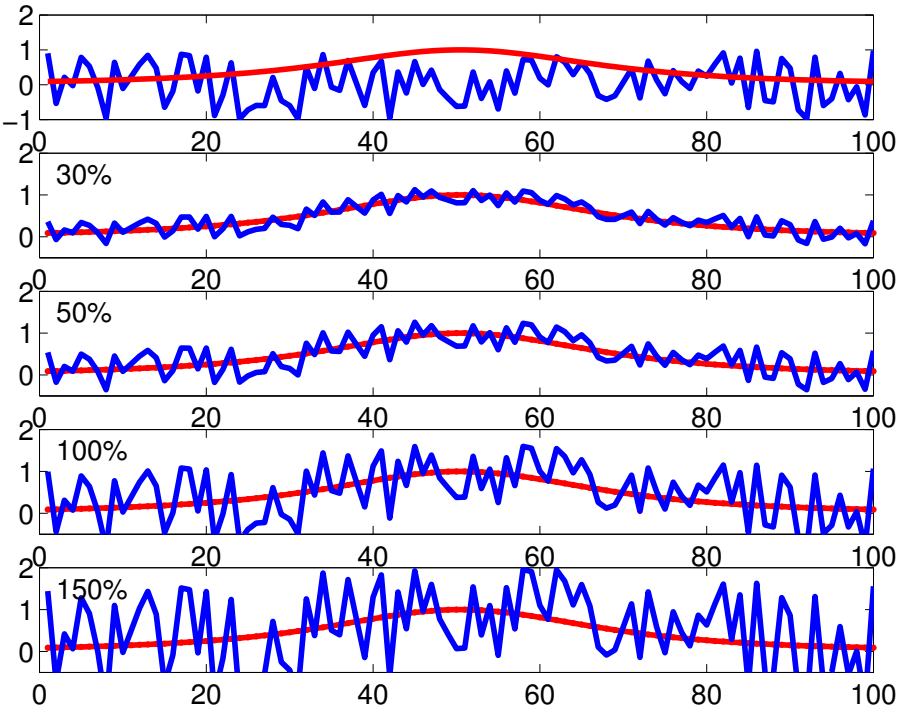

Figure 2: Behaviour of the semblance functions. From top to bottom: Uniform noisy sample with unit amplitude (blue) [$S_1 = 0.01$, $S_2 = 0.01$, $S_4 = 0.01$] and typical amplitude curve (red) [$S_1 = 0.41$, $S_2 = 0.68$, $S_4 = 0.92$]; Amplitude with 25% added noise [$S_1 = 0.34$, $S_2 = 0.61$, $S_4 = 0.88$]; Amplitude with 50% added noise [$S_1 = 0.24$, $S_2 = 0.52$, $S_4 = 0.82$]; Amplitude with 100% added noise [$S_1 = 0.13$, $S_2 = 0.34$, $S_4 = 0.67$]; Amplitude with 150% added noise [$S_1 = 0.10$, $S_2 = 0.24$, $S_4 = 0.53$].

are shown in Figure 2. While the uniform noisy sample itself has indistinguishable values of S_1, S_2 and S_4, the amplitude function is more easily detected as representing a coherent event by the higher semblance value of S_4. Moreover, while all semblance values decrease with increasing noise level, S_4 has the least decrease.

From Figures 1 and 2, we observe that the fourth-order semblance S_4 has the capability of detecting coherency even under a very strong noise. This points towards the potential of an S_4-based semblance analysis to be more successful than standard S_2 analysis in the presence of high levels of noise.

APPLICATION TO CRS STACK

The common reflection surface (CRS) method (see, e.g., Hubral et al., 1998) represents a natural extension of the Commom Midpoint (CMP) method in two important aspects. Firstly, for each stacking trace location (now called simply a central point), the CRS considers a supergather of source-receiver pairs, arbitrarily located with respect to the central point. In other words, the gather is not restricted to the CMP condition. Secondly, not only the stacking velocity, but also other additional parameters are extracted from the data. In the 2D situation, three parameters are determined for each central point and all zero-offset (ZO) traveltime samples. The procedure is performed for all traveltime samples.

To be able to stack traces from source-receiver pairs that do not conform to the CMP condition, the CRS method utilizes the (generalized) hyperbolic moveout,

$$T(x,h) = \sqrt{[T_0 + A\,(x - x_0)]^2 + B\,(x - x_0)^2 + C\,h^2}, \tag{24}$$

where x_0 is the central point, x and h denote the midpoint and half-offset coordinates of the source and receiver pair, and T_0 is the ZO traveltime at the central point. As shown in Hubral et al. (1998), the

parameters A, B and C are related to physical quantities referred to as the CRS parameters or attributes,

$$A = \frac{2\sin\beta}{v_0}, \quad B = \frac{2T_0\cos^2\beta}{v_0}K_N, \quad \text{and} \quad C = \frac{2T_0\cos^2\beta}{v_0}K_{NIP} = \frac{4}{V^2}, \tag{25}$$

where β is the emergence angle of the ZO ray with respect to the surface normal, K_N and K_{NIP} are the curvatures of the N- and NIP-waves, respectively (see Hubral (1983)), and V is the stacking velocity. All these quantities are evaluated at the central point. Finally, v_0 denotes the surface velocity, also at the central point.

The search for the parameters A, B and C can be performed in three main steps. First, for each pair (x_0, T_0), we find the value of the parameter C that maximizes the semblance function (S_1, S_2 or S_4) for the amplitudes along the hyperbolic traveltime within the respective CMP section at x_0. Denoting this CMP section by $\phi(h,t)$, we can write that the vector, $\mathbf{u} = (u_i)$, is given by

$$u_i = \phi(h_i, T_i), \quad \text{with} \quad T_i = T(x_0, h_i) = \sqrt{T_0^2 + C\ h_i^2}, \quad i = 1, 2, \ldots, N_C, \tag{26}$$

where N_C is the number of traces considered inside some aperture. After determination of all parameters, C, the CMP data is stacked. The result of this first-step process is, then, a panel $C(x_0, T_0)$, as well as a stacked section, $\psi(x_0, T_0)$.

The second step consists of the search for parameter A, performed within the stacked section $\psi(x_0, T_0)$. For each pair, (x_0, T_0), we maximize the semblance S_1. S_2 or S_4 of the amplitudes along the hyperbolic traveltime (24) considering $h = 0$ and $B = 0$. In other words, the sample vector, $\mathbf{u} = (u_i)$, is now given by

$$u_i = \psi(x, T_i), \quad \text{with} \quad T_i = T(x, 0) = T_0 + A\ (x - x_0), \quad i = 1, 2, \ldots, N_A, \tag{27}$$

where N_A is again the number of traces considered inside some aperture, now taken in the stacked section. Generally, N_A will be different from N_C. Typically, N_A should be chosen smaller than N_C.

In the third step, to find B, we repeat the search in the stacked section, using the estimated value of A. For each (x_0, T_0), we maximize the semblance for the amplitude vector, $\mathbf{u} = (u_i)$ given by

$$u_i = \psi(x, T_i), \quad T_i = T(x, 0) = \sqrt{[T_0 + A\ (x - x_0)]^2 + B\ (x - x_0)^2}, \quad i = 1, 2, \ldots, N_C. \tag{28}$$

Here, the aperture N_C in the stacked section must be larger than N_A.

NUMERICAL EXPERIMENTS

To compare the behaviour of the different semblance functions in the estimation of CRS parameters and stack, we have applied the procedure described in the previous section to a very simple synthetic data set. The seismic model is depicted in Figure 3. It consists of a smooth reflector below a homogeneous acoustic medium. We analyse the behaviour of the three semblance functions, S_1, S_2 and S_4, for two different central points and also using the correct value of the zero-offset (ZO) (or stacked) time. Also shown in Figure 3 are the two ZO rays at the two central points. For each x_0 we performed one thousand random tests for each of five different sizes of the aperture (number of traces), 10, 20, 30, 50 and 70, and for each of four noise levels, 30%, 50%, 100% and 150%, respectively. An estimate of any parameter A, B or C is considered a success if the deviation from the true value is less than 10%.

Estimation of CRS parameters

The results of the search for parameter C were almost the same in all cases, with no significant advantage of using any of the semblance functions. Parameter C was successfully determined at both points x_0 in over 90% of the tests, even for the highest noise level, with any of the three tested semblance functions. This confirms the well-known robustness of the parameter C.

As opposed to the previous case, significant differences between the success rate for the different semblance functions are now observed in the search for parameter A. Again, we performed one thousand random tests for each of five different sizes of the aperture (number of traces), 10, 20, 30, 50 and 70, and for each of four noise levels, 30%, 50%, 100% and 150%, respectively, at two differerent central points x_0

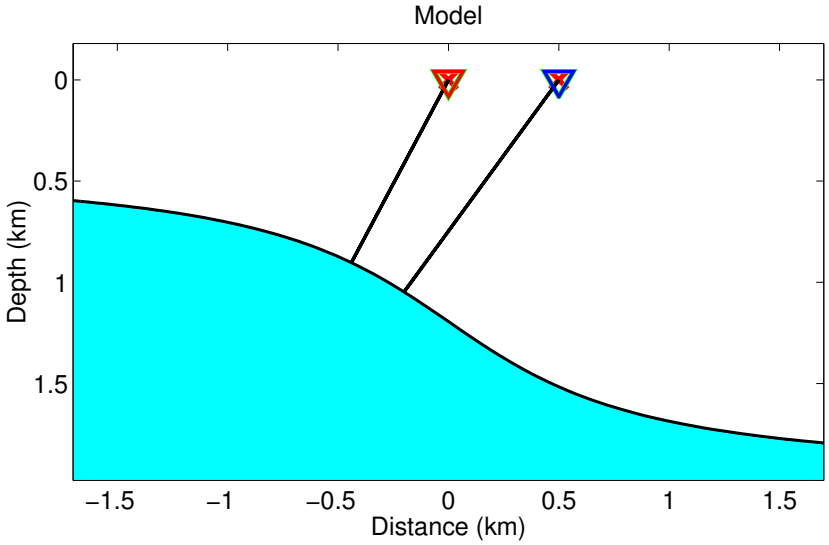

Figure 3: Model and central points for the synthetic experiments.

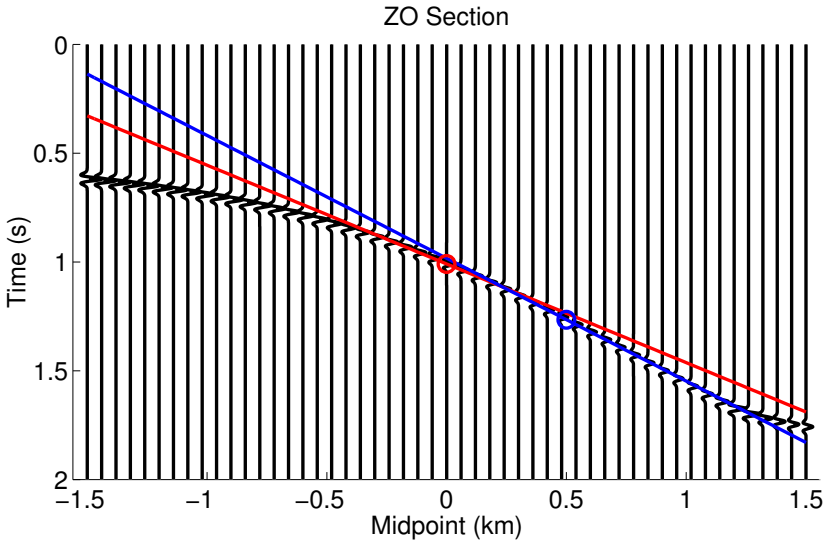

Figure 4: Zero-offset section for the model in Figure 3. Every 3rd trace is shown

in the modeled zero-offset section (see Figure 4). The sought-for results of parameter A at the two central points are the dips of the straight lines tangent to the zero-offset reflection, as depicted in Figure 4.

Figures 5 and 6 depict the percentage of success for parameter A at $x_0 = 5$ km and $x_0 = 0.0$ km, respectively. As can be observed, the search using S_4 has a higher success rate in almost every setting. The largest advantage of the fourth-order semblance function is observed, as expected, at the highest noise level.

Another conclusion from Figures 5 and 6 is that the search for A is highly dependent on the chosen aperture. While there is a high success rate for all aperture sizes at the central point $x_0 = 0$ km, the same is not true at the central point $x_0 = 0.5$ km. The reason is the stronger curvature of the reflection event at $x_0 = 0.5$ km (see again Figure 4), which makes it harder to fit a linear traveltime curve over a larger aperture. Interestingly enough, an aperture of about 20 traces seems to work best at both central points, even though Figure 4 indicates that around $x_0 = 0.5$ km, the traveltime function is approximately linear

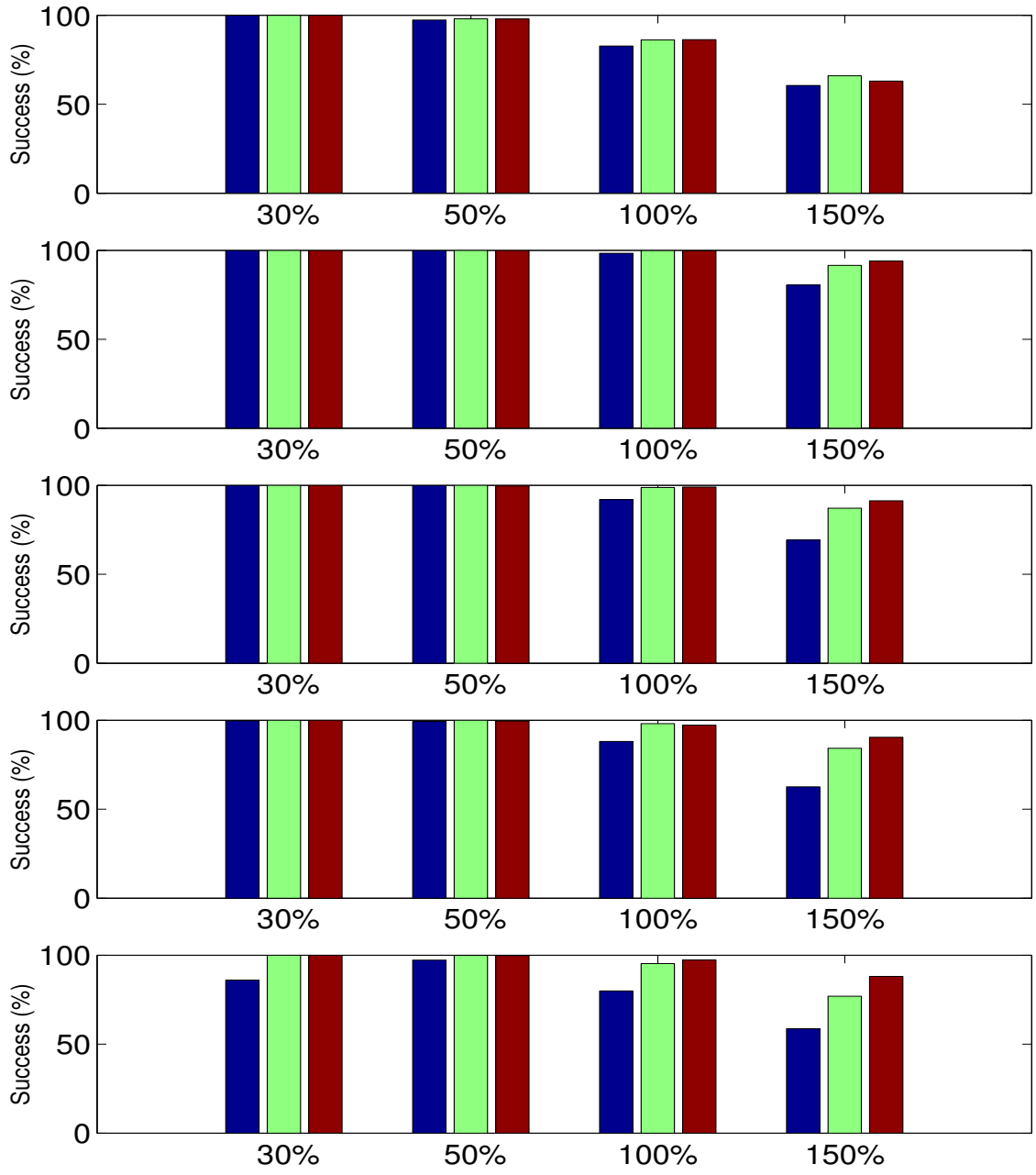

Figure 5: Percentage of success in finding parameter A in the ZO-section for $x_0 = 0.5$ km: S_1 (blue), S_2 (green) and S_4 (red). From top to bottom the number or traces within the aperture increases: 10, 20, 30, 50 and 70. The ratio aperture/depth also increases: 0.3, 0.5, 0.8, 1.0 and 1.5. In the horizontal axis is indicated the level of the added noise: 30%, 50%, 100%, and 150%.

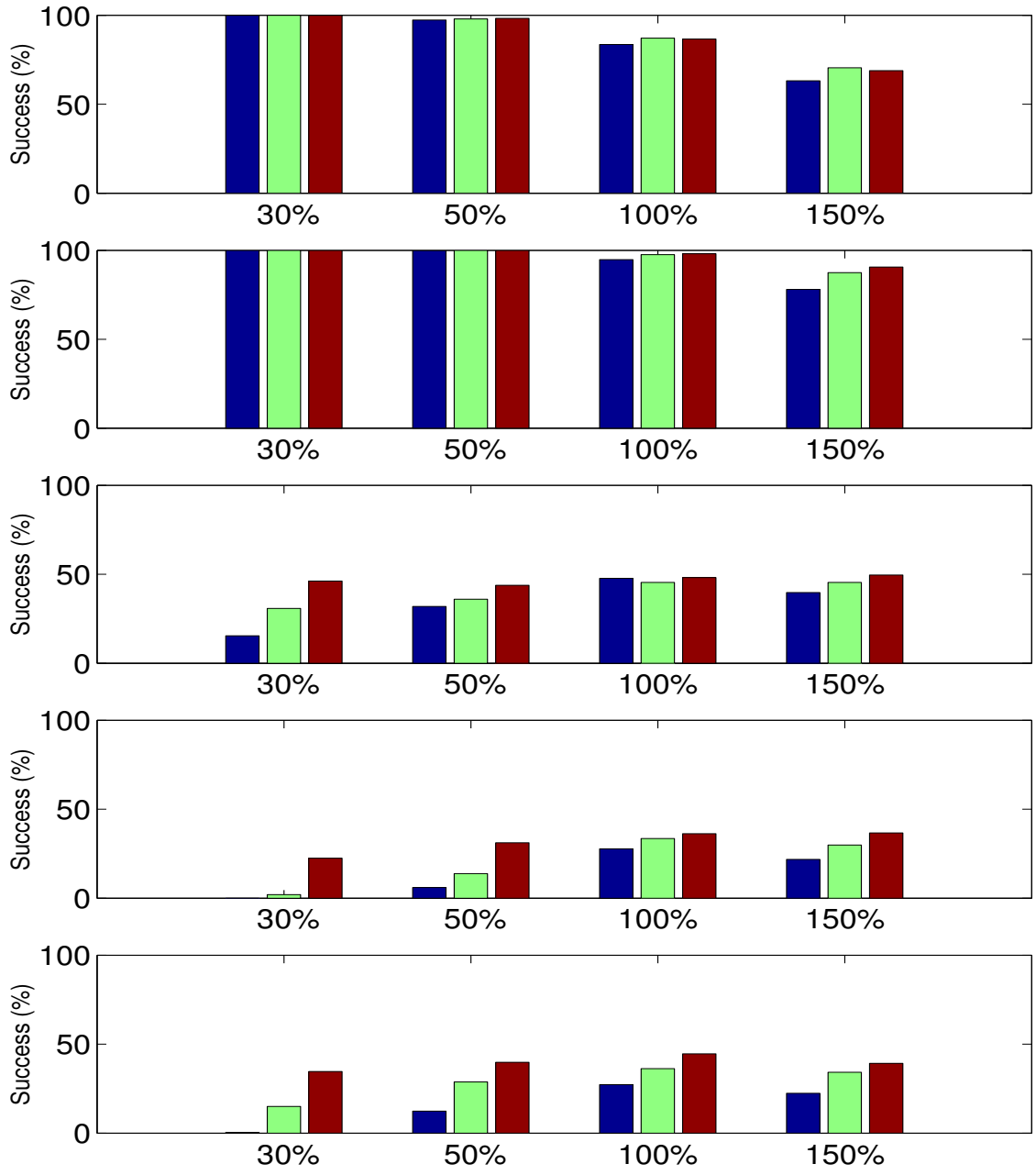

Figure 6: Percentage of success in finding parameter A in the ZO-section for $x_0 = 0.0$ km: S_1 (blue), S_2 (green) and S_4 (red). From top to bottom the number or traces within the aperture increases: 10, 20, 30, 50 and 70. The ratio aperture/depth also increases: 0.3, 0.5, 0.8, 1.0 and 1.5. In the horizontal axis is indicated the level of the added noise: 30%, 50%, 100%, and 150%.

over a larger interval. For this example, the aperture of 20 traces is equivalent to about half the depth of the reflection point.

The final step is the detection of B in the zero-offset section using the estimated values of A. Once more, we performed one thousand random tests for each of five different sizes of the aperture (number of traces), 10, 20, 30, 50 and 70, and for each of four noise levels, 30%, 50%, 100% and 150%, respectively, in the modeled zero-offset section (see Figure 4). Since our interest was in the different performances of the different semblance functions, we carried out the set of experiments using the exact value for A in the search for B in order not to let the error in the estimation of A influence the estimation of B. As in the search for C, we found no significant differences in success rate for B. However, while the search for C was very robust, yielding high success rates for any of the semblance functions, the search for B is rather unstable and the success rates are quite low, particularly for high noise levels. Instability of parameter B is a well-known difficulty encountered by the CRS method.

Behaviour of stacked sections

The second experiment was devised to exemplify the different behaviour of the CRS stacked sections obtained using the different semblance functions. Due to the rather poor performance of S_1 in the statistical tests, and since the standard procedure is to use S_2, we only compare the results using S_2 and S_4. We applied the CRS stacking technique to a complete synthetic dataset for a model with three homogeneous layers separated by one curved and two horizontal interfaces. To study the behaviour of the semblance functions we simulated two types of noise. In the first test, we added white noise of about 60% of the data amplitude. For the second test, we used a lower noise level of about 30%, but convolved it with a Ricker wavelet so as to simulate colored rather than white noise.

Figure 7 shows the CRS stacked sections for the first test data set. The left column shows the results of using S_2 and the right column those of S_4. In the top row, we see the stacked sections after the search for C. Though the first reflector is slightly better visible in the S_4 section, the overall impression is of comparable quality. This is the expected result after the above statistical tests.

In the center row of Figure 7, we see the stacked sections after the search of A. This search is performed in the sections shown in the top row. As expected from the statistical analysis, the search for A was much more successful when using S_4. The second and third reflectors are much better visible in the right panel than in the left one. As the next step, the B values are searched for individually in the center panels. However, because of the small success rate of the B search, the stacked sections do not change much.

The bottom row of Figure 7 shows the final CRS stacked section after a simultaneous search for the best triplet of values A, B, and C. The previously detected individual values of A, B, and C are used as initial values for this search. The higher quality of the right panel is clearly visible. The main reason for the better quality of the final stacked section are the better initial values for the simultaneous search, particularly A. The search itself is rather independent of the choice of the semblance function. Simultaneous search with S_2 using the initial values from the S_4 individual searches results in a stacked section of comparable quality.

Figure 8 shows the corresponding results for the second test with colored noise. While the overall observations remain very similar, we note that even the search for C seems to be more stable with the fourth-order semblance. Apparently, the presence of colored noise in the data is more of a disturbance to a standard S_2 coherence analysis than to the one using S_4.

CONCLUSIONS

In this paper, we have introduced a new fourth-order semblance function. Moreover, we have evaluated its behaviour in CRS parameter estimation and stack. We have seen that the new fourth-order semblance function produces comparable results for the searches of the curvature parameters, but superior results for the linear search. The fourth-order measure is less dependent on aperture and noise level, thus resulting in reliable estimates of the local slope more often than when using conventional semblance. As a consequence, the fourth-order-semblance based final CRS stack after the whole search procedure is of better quality than the corresponding one based on second-order semblance stack.

Another conclusion from our analysis is that the linear search is highly dependent on the chosen aper-

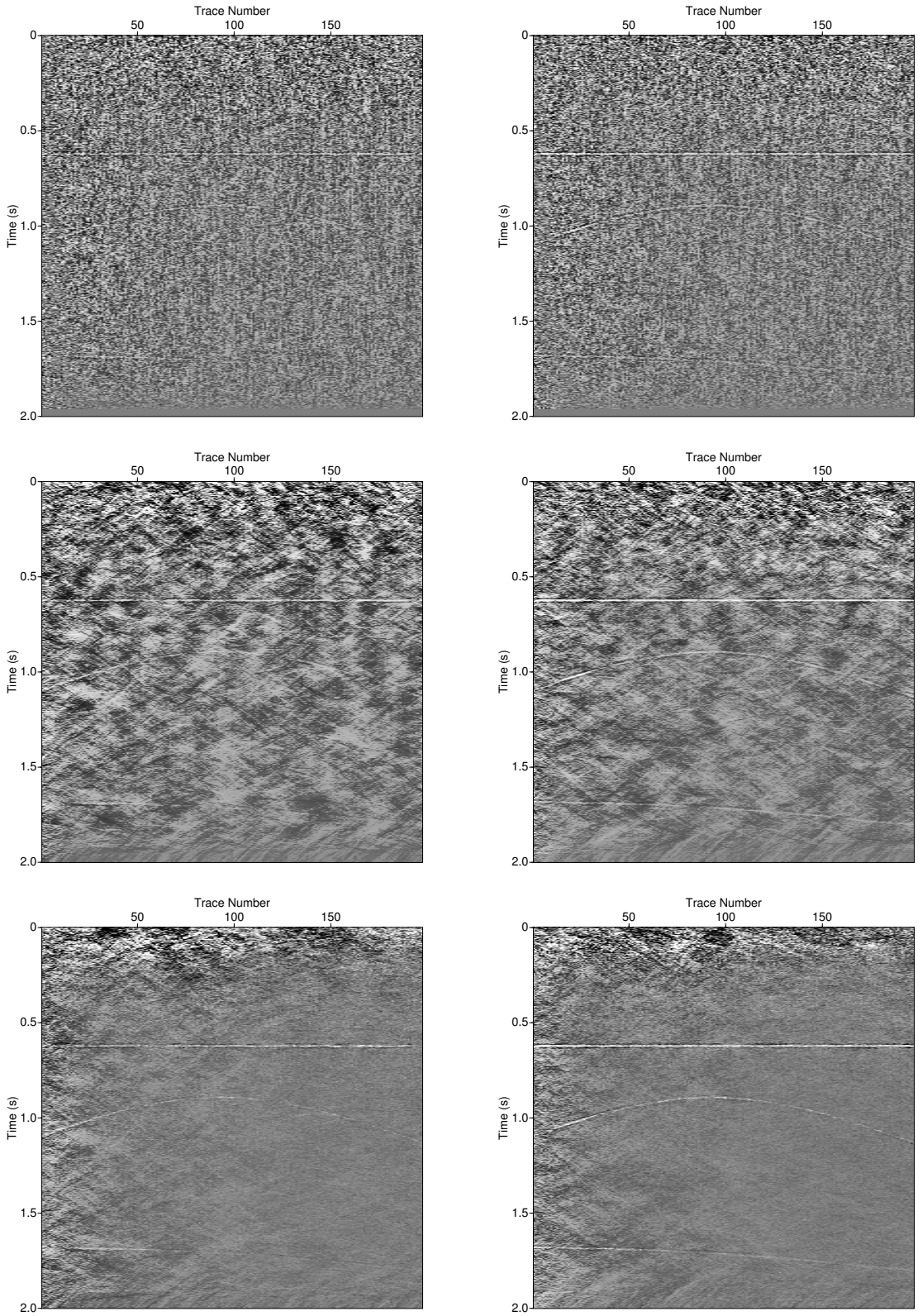

Figure 7: Stacked sections after the searches, with 60% white noise. Top: C. Center: A. Bottom: Simultaneous. Left: S_2. Right: S_4.

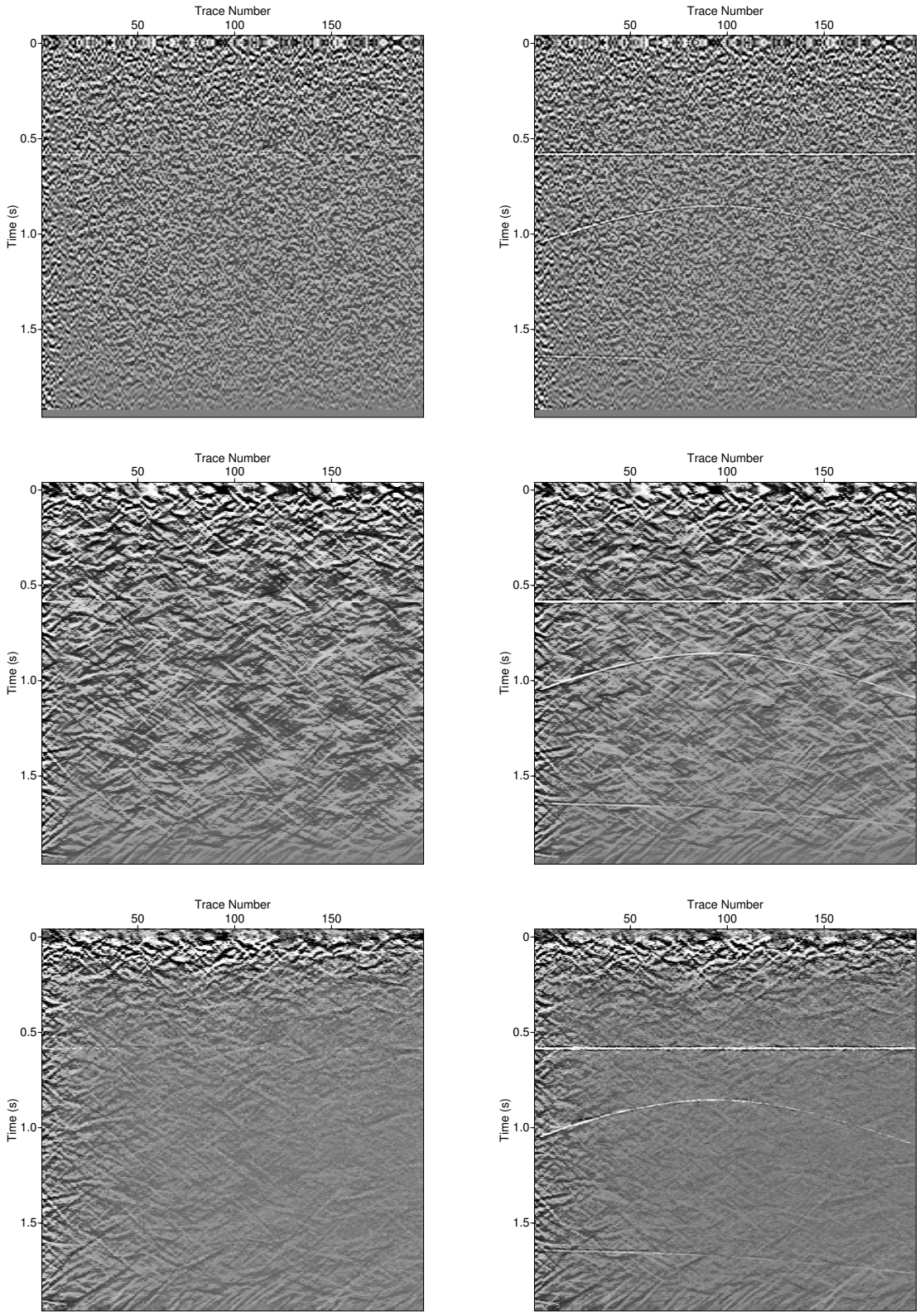

Figure 8: Stacked sections after the searches, with 30% colored noise. Top: C. Center: A. Bottom: Simultaneous. Left: S_2. Right: S_4.

ture. Depending on the curvature of the reflection event in the stacked section, the success rate can decrease dramatically with increasing aperture. For our examples, an aperture of about half the depth of the reflection point produced the best results.

ACKNOWLEDGEMENTS

This work was kindly supported by the *National Council of Scientific and Technological Development (CNPq)*, Brazil, and the sponsors of the *Wave Inversion Technology (WIT) Consortium*, Germany.

REFERENCES

Al-Yahya, K. M. (1989). Velocity analysis by iterative profile migration. *Geophysics*, 54(06):718–729.

Doherty, S. M. and Claerbout, J. F. (1976). Structure independent velocity estimation. *Geophysics*, 41(5):850–881.

Dohr, G. P. and Stiller, P. K. (1975). Migration velocity determination - part ii: Applications. *Geophysics*, 40(1):6–16.

Douze, E. J. and Laster, S. J. (1979). Statistics of semblance. *Geophysics*, 44(12):1999–2003.

Höcht, G., de Bazelaire, E., Majer, P., and Hubral, P. (1999). Seismics and optics: hyperbolae and curvatures. *J. Appl. Geoph.*, 42(3/4):261–281. Special Issue on "Macro-Model Independent Seismic Reflection Imaging".

Hubral, P. (1983). Computing true amplitude reflections in a laterally inhomogeneous earth. *Geophysics*, 48:1051–1062.

Hubral, P., Höcht, G., and Jäger, R. (1998). An introduction to the common reflection surface stack. *60th EAGE Conference & Exhibition, Expanded Abstracts*, Session:01–19.

Müller, T. (1999). *The Common Reflection Surface Stack Method*. PhD thesis, Universität Karlsruhe (TH).

Reiter, E. C., Toksöz, M. N., and Purdy, G. M. (1993). A semblance-guided median filter. *Geophysical Prospecting*, 41(1):15–42.

Sattlegger, J. W. (1975). Migration velocity determination: Part I. Philosophy. *Geophysics*, 40(1):1–5.

Schleicher, J. and Biloti, R. (2007). Dip correction for coherence-based time migration velocity analysis. *Geophysics*, 72(1):S431–S48.

Symes, W. W. and Carazzone, J. J. (1991). Velocity inversion by differential semblance optimization. *Geophysics*, 56(5):654–663.

Symes, W. W. and Kern, M. (1994). Inversion of reflection seismograms by differential semblance analysis: Algorithm structure and synthetic examples. *Geophysical Prospecting*, 42(6):565–614.

Taner, M. T. and Koehler, F. (1969). Velocity spectra - digital computer derivation and application of velocity function. *Geophysics*, 34:859–881.

Yilmaz, O. (1979). *Prestack Partial Migration*. PhD thesis, Stanford University.